Int. J. Electrochem. Sci., 10 **(2015)** 2391 - 2399

International Journal of
ELECTROCHEMICAL
SCIENCE
www.electrochemsci.org

Photoluminescence and Optoelectronics Characteristics of Eu-doped $InBO_3$ Nanocrystals

Zhe-Wei Chiu[1], *Yu-Jen Hsiao*[2], *Te-Hua Fang*[1,*], *Liang-Wen Ji*[3]

[1] Department of Mechanical Engineering, National Kaohsiung University of Applied Sciences, Kaohsiung 807,Taiwan
[2] National Nano Device Laboratories, National Applied Research Laboratories, Tainan 741, Taiwan
[3] Institute of Electro-Optical and Materials Science, National Formosa University, Yunlin 632, Taiwan
[*]E-mail: fang.tehua@msa.hinet.net

Received: 22 August 2014 / *Accepted:* 6 January 2015 / *Published:* 19 January 2015

Indium boron oxide($InBO_3$) nanocrystals doped with Eu^{3+} ions prepared via the sol-gel method are characterized. The photoluminescence spectra excited at 263 nm have a strong red emission band with a peak at 616 nm. The $^5D_0 \rightarrow {}^7F_1$ (593 nm) and $^5D_0 \rightarrow {}^7F_2$ (616 nm) transitions of Eu^{3+} appear at a quenching concentration of above 5 mol%. The optical absorption spectra of the Eu-doped host annealed at 700 °C exhibit a band-gap energy of 5.05 eV. It is found that $InBO_3$:xEu (x= 5 mol%) added to a hybrid solar cell improves the short-circuit current density and increases the photoelectric conversion efficiency to 1.88%.

Keywords: Nanostructures, Sol-gel growth, Photoluminescence, Optical properties.

1. INTRODUCTION

Rare-earth (RE)-doped materials have received a lot of attention for application in next-generation flat-panel displays and solar cells. Indium boron oxide is an attractive host material for bright scintillators and nanophosphors. RE-doped host materials have been found to exhibit luminescence. For example Gd_2O_3 doped with Dy^{3+} can transfer from green to write light. Europium-doped lanthanum oxychloride nanophosphor provide excellent red colors for monitors [1-4].

Recently, many Eu^{3+}-doped materials have been extensively studied due to the intra-4f-shell transitions that occur from the excited level down to the lower levels: $^5D_0 \rightarrow {}^7F_j$ (j = 1, 2, 3, 4) for Eu^{3+} ions [5-7]. The emission intensity is dominated by wavelength peaks in the range of 610-630 nm.

Solar energy has received a lot of attention as a renewable energy source. The absorption wavelength of a general solar cell is between about 400 and 1000 nm. $InBO_3$ doped with Eu^{3+} used as

an optical wavelength conversion layer can absorb a portion of the incident solar radiation and re-emit part of it at lower energies, thus producing a spectral down-shift that enhances the efficiency of solar cells [8]. The photoluminescence of $InBO_3$ doped with Eu^{3+} is very promising for application to solar cells because the excitation wavelengths are shorter than 400 nm.

$InBO_3$ has a hexagonal unit cell and is isostructural with calcite [9]. $InBO_3$ photocatalyst with a calcite structure has been used for water splitting via a solid-state reaction and a two-step precipitation method [10]. Jyotsna Thakur reported a gel-combustion method for preparing $InBO_3$:Eu with multiband orange–red luminescence: the technique has short processing, and produces high-purity single- or multi-phase complex oxide powders [11]. The sol-gel method requires the lowest temperature of processes used to obtain pure $InBO_3$. The major advantages of the sol–gel process are: (i) high purity of precursors, (ii) ambient temperature for sol preparation and gel processing, (iii) product homogeneity, (iv) low-temperature sintering, and (v) good control of particle size and particle size distribution [12].

The present study synthesizes $InBO_3$:Eu with a small particle size and high red color purity via the sol-gel method. Poly(3-hexylthiophene):(6,6)-phenyl-C61-butyric acid methyl ester (P3HT:PCBM)/$InBO_3$:xEu hybrid films are prepared for organic photovoltaics (OPVs). In addition, InBO3:xEu nanocrystal is embedded in P3HT and PCBM for enhancing the efficiency of hybrid organic solar cells. The effects of dopant content on the morphology, optical absorption, photoluminescence, and photovoltaic performance of OPVs are investigated.

2. EXPERIMENTS

$InBO_3$:Eu powders were prepared via the sol-gel method using indium(III) nitrate, 99.9% ($In(NO_3)_3$, tri-n-butyl borate, 98% ($C_{12}H_{27}BO_3$), citric acid (CA, $C_6H_8O_7$), and europium nitrate ($Eu(N_3O)_9{\cdot}5H_2O$) as starting materials. First, stoichiometric amounts of indium nitrate and tri-n-butyl borate were dissolved in distilled water. A sufficient amount of citric acid was then added to the former solution as a chelating agent. A citric-acid-to-total-metal-ion molar ratio of 1:1 was used. The precursor was dried in an oven at 120 °C for 10 hr. The powders were obtained after calcination at 700 °C for 3 hr in air. The phases were identified using X-ray powder diffraction (XRD, Rigaku Dmax-33). The surface morphology and microstructure were examined by high-resolution transmission electron microscopy (HRTEM). The excitation and emission spectra were measured by a fluorescence spectrophotometer (Jasco FP-6600) equipped with a xenon lamp at room temperature. The absorption spectra were measured using an ultraviolet-visible (UV-Vis) spectrophotometer (Hitachi, U-3010).

The hybrid organic solar cells were fabricated on indium tin oxide (ITO)-coated glass substrates. The active layer consisted of poly(3- hexylthiophene) (P3HT, FEM. Inc.) and [6,6]-phenyl-C61-butyric acid methyl ester (PCBM, Nano-C) dissolved in 1,2-dichlorobenzene (DCB) (with 10:8 wt% P3HT:PCBM) with 0.5 wt% $InBO_3$:xEu (x=5 mol%) nanocrystals. The hybrid solar cell of the photoactive absorber P3TH:PCBM:$InBO_3$:Eu film was spin-coated onto 300-nm-thick indium tin oxide (ITO)/poly(3,4-ethylendioxythiophene): poly(styrenesulfonate) (PEDOT:PSS) substrates. The substrates were then annealed at 120 °C for 1 min. Finally, a 120-nm-thick Ca/Al electrode was

deposited onto the active layer through a shadow mask by thermal evaporation. The current–voltage measurements (Keithley 2410 source meter) were obtained using a solar simulator (TELTEC) with an air mass (AM) 1.5 filter under an irradiation intensity of 100 mW/cm^2.

3. RESULTS AND DISCUSSION

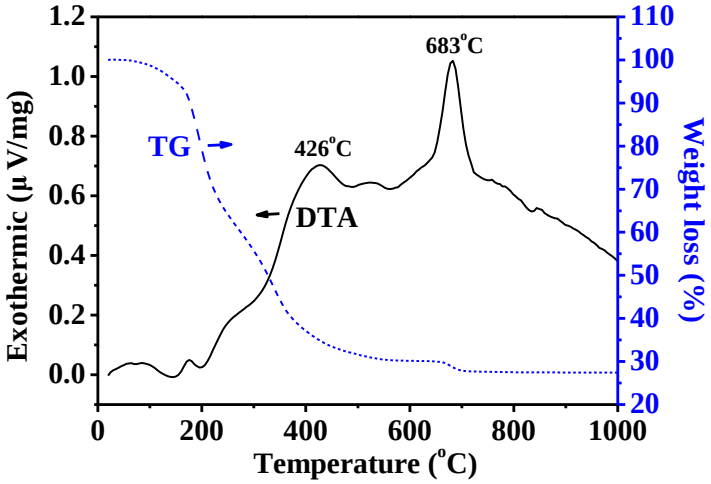

Figure 1. DTA and TGA curves for $InBO_3$ precursor.

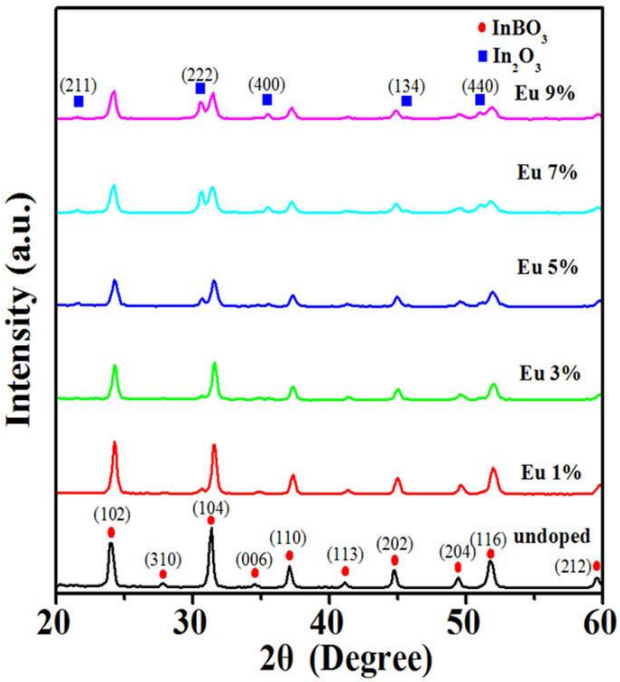

Figure 2. XRD patterns of $InBO_3$:xEu powders annealed at 700 °C for 3 hr (x= 0, 1, 3, 5, 7, and 9 mol%).

Differential thermal analysis (DTA) and thermogravimetry analysis (TGA) curves of the dry $InBO_3$ precursor are shown in Fig.1. Exothermic peaks appear at about 426 °C and 683 °C, respectively. The crystallization temperature is 683 °C. The endothermic peak at about 130 °C in DTA

accounted for 6% of the initial weight loss in TG, and was assigned to the loss of free water. There is a weight loss of about 58.3 % in the range of 180-562 °C, which contains exothermic peaks at 426 and 522 °C. The exothermic peak at 426 °C was due to the burnout of the low boiling organic species, and that at 522 °C originated from the burnout of the organic groups in citric acid. An exothermic peak appears around 683 °C, which is associated with the decomposition of the amorphous gel into the crystalline phase.

Figure 2 shows the XRD patterns of $InBO_3$ doped with various concentrations of Eu^{3+}. The figure shows that the pure $InBO_3$ phase has a hexagonal structure at 700 °C (JCPDS Card No.17-0933). There is a second phase of cubic crystals with In_2O_3 (JCPDS Card No.06-0416). All the peaks can be well-indexed to pure $InBO_3$ for heat-treatment temperatures of over 700 °C. Eu^{3+} ions can replace In^{3+} ions. The Eu^{3+} contains about 7 mol% has some residual indium oxide. The Eu^{3+} ion is able to replace In^{3+}. Note that the intensity of the diffraction peaks increases with decreasing Eu doping concentration. An increase in Eu doping decreases the crystallinity of $InBO_3$. The radii of B^{3+}, In^{3+}, and Eu^{3+} ions are 0.28, 0.81, and 0.95 Å, respectively. When Eu^{3+} ions are doped into $InBO_3$, the Eu^{3+} ions occupy In^{3+} ion sites [13]. The mechanism of formation of this solid solution reaction is:

$$In(NO_3)_3 + C_{12}H_{27}BO_3 + Eu(NO_3)_3\ 5H_2O \rightarrow In_{1-x}(Eu)_xBO_3 + 5NO_2\uparrow + 17H_2O\uparrow + 12CO_2\uparrow + NH_3\uparrow \quad (1)$$

Figure 3 (a) shows a low-magnification TEM image that shows the morphology of a sample annealed at 700 °C. The diameters of the nanocrystals are in the range of 20–100 nm. A high-magnification TEM image and the selected area electronic diffraction (SAED) pattern of the nanocrystals are shown in Fig. 3 (b). It is believed that the assemble effect arising from the nanocrystals is responsible for the decrease in surface energy. The interplanar distance of the crystal fringes is 0.22 nm. As shown in the inset of Fig. 3 (b), the SAED pattern of the sample is consistent with the high crystallization of $InBO_3$:xEu (x=5 mol%).

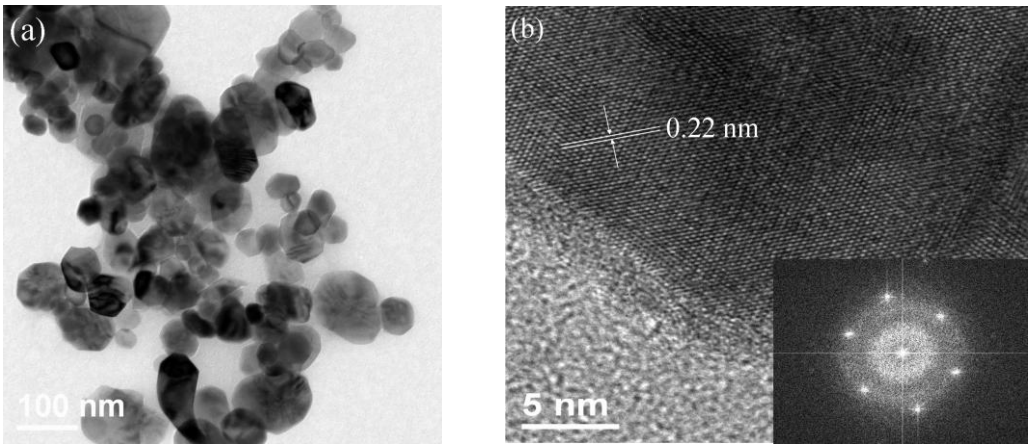

Figure 3. TEM images of $InBO_3$:xEu (x=5 mol%) as-synthesized nanocrystals annealed at 700 °C, and (b) HRTEM image and electron diffraction pattern of the nanocrystals.

The host prepared has a strong ultraviolet emission band centered at 306 nm and excitation at 263 nm can be observed for pure $InBO_3$, the change transfer process from O^{2-} to In^{3+} of the host. The grain size influences the emission properties decreasing the surface area of the host [14].

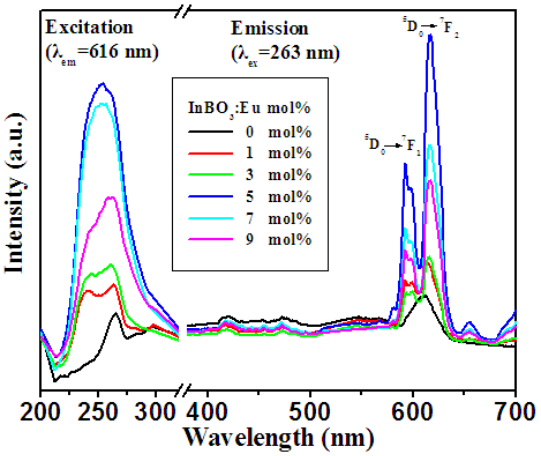

Figure 4. Room-temperature excitation (λem=616 nm) spectra and emission (λex=263 nm) spectra of $InBO_3$ phosphors doped with various concentrations of Eu annealed at 700 °C for 3 hr.

Figure. 4 shows the excitation spectra and emission spectra of the $InBO_3$ phosphors doped with various concentrations of Eu (0, 1, 3, 5, 7, and 9 mol%) annealed at 700 °C for 3 hr. The intensity of the luminescence increased with increasing Eu concentration for concentrations up to about 5 mol%, and then abruptly decreased. This behavior can be explained by: (1) an increased defect density in the sample with a higher Eu concentration and (2) the concentration quenching effect [15,16]. However, increasing the dopant concentration up to C_{Eu} =5% led to an increase in the peak intensity at the $^5D_0$-$^7F_1$ and $^5D_0$-$^7F_2$ spectral site. This can be attributed to the crystal field results. The emission behavior of Eu^{3+} ions is affected by the crystal field, so that more than one emission mechanism is introduced in biphase crystallites. The second phase In_2O_3 aggregate increases the number of Eu atoms occupying the noncentrosymmetric and centrosymmetric sites, increasing emission intensity. As more Eu^{3+} ions are incorporated into pure $InBO_3$, a second phase precipitates, so the change of coulomb attraction force causes the activator (Eu^{3+}) to experience different crystal fields, leading to a decrease in the emission spectra [17]. In this study, some Eu^{3+} ions may have stacked on the sites out of the host and led to the emission spectra increase.

The excitation spectra of $InBO_3$:Eu phosphor consist of a broad band from 220 to 310 nm with a peak at about 263 nm. The emission curve shows emission peaks at about 593 and 616 nm. The emission spectra are dominated by the transitions of $^5D_0 \rightarrow ^7F_1$ (593 nm) and $^5D_0 \rightarrow ^7F_2$ (616nm) [18]. The photoluminescence results reveal that the sample prepared with 5 mol% Eu had the highest red emission peak at 616 nm.

The emission behavior may have been caused by the variable nature of the surrounding medium between the second phase and the crystalline structure. The decrease in the lifetime when the doped concentration was increased can be attributed to the non-radiative relaxation caused by the surface defects that act as a quenching center. When the doped concentration was increased, the

sample had more and more quenching centers and the non-radiative rate increased, which caused the lifetime to be shortened. [19]

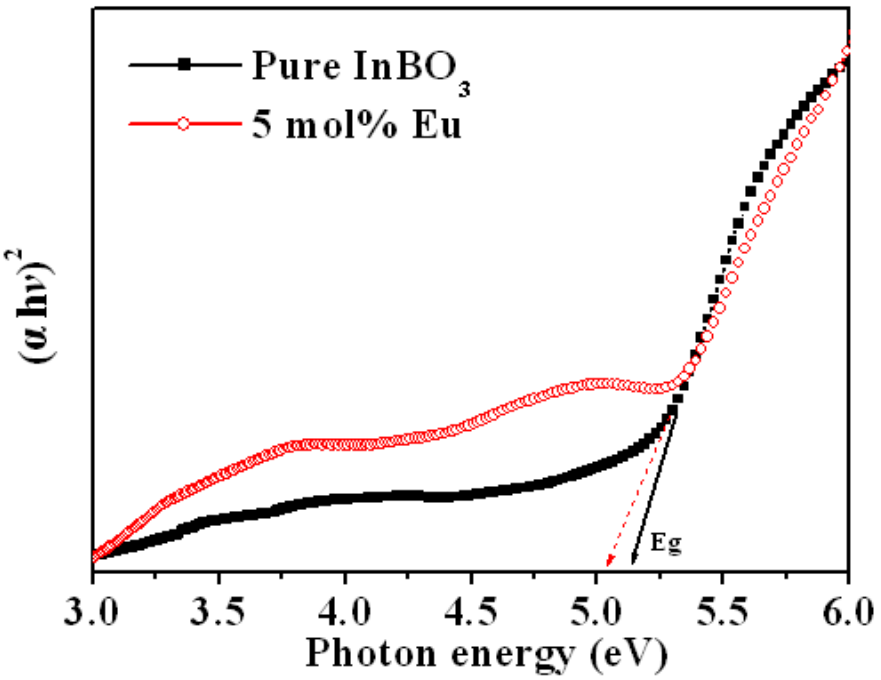

Figure 5. Optical absorption spectra of hosts doped with Eu^{3+} annealed at 700 °C for 3 hr.

The optical absorption spectra of $InBO_3$ and $InBO_3$:xEu powders annealed at 700 °C for 3 hr are shown in Fig. 5. The optical absorption is a function of photon energy of pure $InBO_3$ and $InBO_3$:xEu. For a direct-band-gap semiconductor, the absorption coefficient in the vicinity of the onset due to the electronic transition is given by [20]:

$$\alpha = \frac{C(hv - Eg)^{\frac{1}{2}}}{hv} \quad (2)$$

where α is the absorption coefficient, *C* is a constant, *hv* is the photon energy, and *E*g is the band gap. Figure 5 shows the relationship of $(\alpha hv)^2$ and photon energy. The visible-light absorption edges of undoped and Eu-doped $InBO_3$ samples are at 5.15 and 5.05 eV, respectively, which are close to the 5.4 eV obtained for samples prepared using a solid-state reaction and a two-step precipitation method [10]. Pure $InBO_3$ was more insulating than $InBO_3$:Eu at a given sintering temperature. The extra absorption peak about at 4.7 eV may be caused by the absorption of defect levels in $InBO_3$:Eu [21].

The emission lifetime was measured at 263 nm excitation and 616 nm emission at room temperature. The decay time τ is about 1.54 ms for InBO3:xEu (x=5 mol%) nanophosphor for the $^5D_0 \rightarrow {}^7F_1$ emission of Eu^{3+}, which is within the range of reported values of 0.62 to 2.64 ms [1, 22].

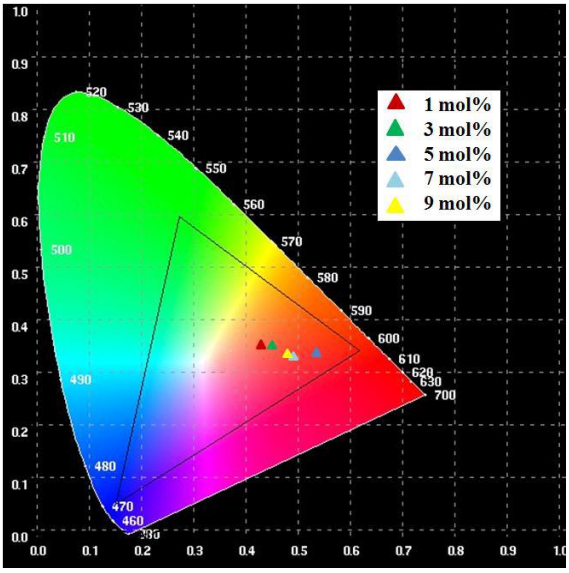

Figure 6. CIE color coordinate diagram of InBO3:xEu phosphors. x = 1, 3, 5, 7, 9 mol%.

The Commission International de l'Eclairage (CIE) chromaticity coordinates of the $InBO_3$ crystalline doped with various concentrations of Eu^{3+} at λ_{ex}=263 nm were measured. When the doping level was changed from 1 mol% to 5 mol%, the CIE color coordinates shifted from X = 0.425 and Y = 0.359 to X = 0.528 and Y = 0.343, which represents a shift from orange to red show in figure 6. When the doping level was changed from 5 mol% to 9 mol%, the CIE color coordinates shifted from X = 0.528 and Y = 0.343 to X = 0.482 and Y = 0.330, which represents a shift from red to pink. When phorphos standing time form 12 to 240 hr, the CIE color coorimates was no obvious change, it show $InBO_3$:xEu (x=5 mol%) of the time with good color stability.

4. HYBRID SOLAR CELL APPLICATION

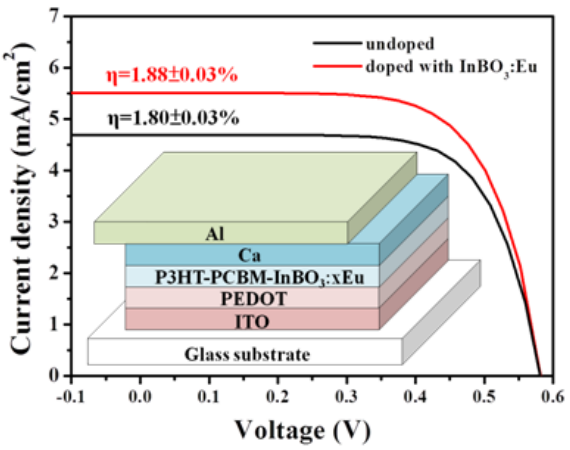

Figure 7. Short-circuit current - voltage curves of hybrid solar cell with 0.5 wt% $InBO_3$:xEu (x=5 mol%) nanostructure blend of P3HT and PCBM. Inset shows the structure of the solar cell device.

Reference devices were produced by spin-coating as-received PEDOT:PSS and P3HT:PCBM in a 1:0.8 ratio dissolved in 1,2-dichlorbenzene (DCB). The inset in Fig. 7 shows a schematic diagram of the hybrid solar cell. The generated electron-hole pairs are separated at the PEDOT/P3HT-PCBM-$InBO_3$:xEu interface. The work function of $InBO_3$:xEu (x=5 mol%) is close to that of an ITO electrode. The hybrid nanophosphor of P3HT-$InBO_3$:xEu (x=5 mol%)-PEDOT-ITO improves the hole mobility of solar cells [23]. The current-voltage (I-V) measurements are plotted in Fig. 6. The photovoltaic properties of the hybrid solar cells with nanostructures are shown in Table 1.

Table 1. Photovoltaic parameters of hybrid solar cells with nanostructures.

Sample	V_{oc} (V)	J_{sc} (mA/cm^2)	FF (%)	η (%)
Pure $InBO_3$	0.5799	4.69	66.32	1.80
$InBO_3$:Eu	0.5799	5.47	59.26	1.88

FF: fill factor; η: power conversion efficiency

$InBO_3$:Eu increased electron-hole separation and the short-circuit current density. The $InBO_3$:xEu nanoparticles act as a scattering layer, which can lead to better absorption via optical confinement within the active layer of the device. The scattering can also enhance power conversion efficiency [24]. Nanophosphor $InBO_3$:xEu (x=5 mol%) absorbed UV light at about 263 nm and showed strong red emission peaks at about 593 and 616 nm. This means that the phosphor enhances the absorption of OPVs in the red wavelength band. The external quantum efficiency (EQE) spectra of the P3HT:PCBM blend is highly conversion efficiency at 300 to 650 nm [25]. The P3HT:PCBM interface increased the absorption of wavelengths in the range of 580 to 640 nm, which increased the short-circuit current density and thus the conversion efficiency. The measurements reveal that a small amount of $InBO_3$:Eu embedded into the P3HT:PCBM photoactive film increased the short-circuit current density from 4.69 to 5.47 mA/cm^2. The power conversion efficiency of the device improved from 1.80% to 1.88%.

5. CONCLUSION

$InBO_3$:Eu nanophosphors were mixed into a P3HT/PCBM polymer matrix. A series of Eu^{3+}-doped $InBO_3$ nanocrystals was synthesized via the sol-gel method at 700 °C. $InBO_3$ shows broad and strong red emission with a peak at 616 nm, which is attributed to the $^5D_0 \rightarrow {}^7F_2$ transition. The optimum concentration of Eu^{3+} is 5 mol%. $InBO_3$:Eu can be a wavelength conversion phosphor for ultraviolet to red wavelengths for OPVs. The power conversion efficiency of the devices improved from 1.80 to 1.88%, resulting in an increased current density when the InBO3:xEu (x=5 mol%) concentration at 0.5 wt%.

ACKNOWLEDGEMENT
This study was financially supported by the Ministry of Science and Technology, Taiwan under grants MOST 103-2221-E-151-001-MY3.

References

1. Q. Xiao, Y. Liu, L. Liu, R. Li, W. Luo, X. Chen, *J. Phys. Chem*. C. 114 (2010) 9314-9321.
2. A. Choubey, S. Som, M. Biswas, S.K. Sharma, *J. Rare Earths*. 4 (2011) 345-348.
3. M. Jayasimhadri, B.V. Ratnam, K. Jang, H.S. Lee, S.S Yi, J.H. Jeong, *Thin Solid Films*. 518 (2010) 6210-6213.
4. K. Mishra, N.K. Giri, S.B. Rai, *Appl. Phys*. *B* 103 (2011) 863-875.
5. J.S. Lee, S.J. Kim, T.K. Kim, R.K. Singh, *J. Mater. Res.* 24 (2009) 2584-2588.
6. P. Chen, X. Ma, D. Yang, *J. Alloys Compounds*. 431 (2007) 317-320.
7. G. Ehrhart, M. Bouazaoui, B. Capoen, V. Ferreiro, R. Mahiou, O. Robbe, S. Turrell. *Optical Mater*. 29 (2007) 1723-1730.
8. Y.J Hsiao, T.H. Fang, L.W. Ji. *Mater. Lett*. 64 (2010) 2563-2565.
9. N.G. Kononova, A.E. Kokh, T.B. Bekker, P.P. Fedorov, E.A. Tkachenko. *Inorganic Mater*. 11 (2004) 1208-1210.
10. Q. Jia, Y. Miseki, K. Saito, H. Kobayashi, A. Kudo. *Bull. Chem. Soc. Jpn*. 83 (2010) 1275.
11. J. Thakur, D. P. Dutta, H. Bagla, A. K. Tyagi. *J. Am. Ceram. Soc*. 95 [2] (2012) 696-704.
12. Y.J. Hsiao, Y.H. Chang, Y.S. Chang, T.H. Fang, *J. Am. Ceram. Soc*. 90 (2007) 2287-2290.
13. B. S. Tsai, Y. H. Chang, Y. C. Chen. *Electrochemical and Solid-State Letters*. 8 (2005) H55-H77.
14. Z. W. Chiu, T.H. Fang, Y. J. Hsiao. *J. Luminescence*. 132 (2012) 2608-2611.
15. W. J. Miniscalco. *J. Lightwave Technol*. 9 (1991) 234-250.
16. B. S. Tsai, T. H. Chang, Y. C. J.Chen. *Mater. Res*. 19 (2004) 1504-1508.
17. A. H. Kitai. Solid State Luminescence, London: Chapman & Hall. (1993).
18. T.H. Fang, Y.S. Chang, L.W. Ji, S.D. Prior, W. Water, K.J. Chen, C.F. Fang, C.N. Fang, S.T. Shen. *J. Phys. Chem. Solids*. 70 (2009) 1015-1018.
19. L. Ozawa, H. Forest, P.M. Jaffe, G. Ban, *J. Electrochem. Soc*. 118 (1971) 482-486.
20. Y.J. Hsiao, C.W. Liu, B.T. Dai, Y.H. Chang, *J. Alloys Compounds*. 475 (2009) 698-701.
21. Y.J. Hsiao, T.H. Fang, S.J. Lin, J.M. Shieh, L.W. Ji, *J. Luminescence*. 130 (2010) 1863-1865.
22. T.H. Fang, Y. J. Hsiao, Y. S. Chang and Y. H. Chang. *Materials Chemistry and Physics*. 100 (2006) 418-422.
23. Y. Y. Yu, W. C. Chien, Y. H. Ko, Y. C. Chan, S. C. Liao, *Current Applied Physics*. (2012) 1-7.
24. V. Kruefu, E. Peterson, C. Khantha, C. Siriwong, S. Phanichphant, D. L. Carroll. *Applied Physics Letters*. 97 (2010) 053302.
25. E. Voroshazi, B. Verreet, T. Aernounts, P. Heremans, *Solar Energy Materials and Solar Cells*. 95 (2011) 1303-1307.